

# Analysis of regenerated cellulose fibers with ionic liquids as a solvent as spinning speed is increased

Guansen Jiang · Ye Yuan · Baochun Wang ·  
Xuemin Yin · Kanukai Susan Mukuze ·  
Weifeng Huang · Yumei Zhang · Huaping Wang

Received: 26 December 2011 / Accepted: 24 April 2012 / Published online: 6 May 2012  
© Springer Science+Business Media B.V. 2012

**Abstract** In order to improve the spinning efficiency, the spinning experiments with cellulose/1-butyl-3-methylimidazolium chloride solution were done whilst increasing spinning speed. It was found that the tenacity and initial modulus of regenerated cellulose fibers increased but the elongation at break decreased slightly with increasing spinning speed at constant draw ratio. Further, the synchrotron wide-angle X-ray diffraction and small-angle X-ray scattering were carried out to illustrate the relationship between the structure and the mechanical properties. It was shown that the crystal orientation, crystallinity, amorphous orientation factor as well as orientation of the microvoids along the fiber increased with the spinning speed as the diameter of the microvoids in the fiber decreased. From the analysis of the spinline stress, it is clear that the spinline stress increased when both extruding and draw speed increased at constant draw ratio. This resulted in the improvement of supramolecular structure and mechanical properties of the regenerated cellulose fibers.

**Keywords** Cellulose fiber · Ionic liquid · Spinning speed · Structure and property

## Introduction

Since Swatloski et al. (2002) first reported that ionic liquids (ILs) could be used as a novel nonderivitizing solvent for cellulose, the dissolution and spinning of cellulose with ILs as solvent have attracted a lot of research interest (Hermanutz et al. 2006; Cuissinat et al. 2008). Based on the spinning technology of Lyocell fibers, regenerated cellulose fibers with a high tenacity of 4.29 cN/dtex were prepared by Laus et al. (2005) with the solvent 1-butyl-3-methylimidazolium chloride ([BMIM]Cl). The dissolution and spinning of cellulose in several ILs with different anion and cation structure were investigated by Kosan et al. (2008). They concluded that cellulose in ILs exhibit good spinnability and fibers with tenacity as high as 5.34 cN/dtex was obtained. Cai et al. (2010) studied the relationship between the spinning technology, the structure and properties of regenerated cellulose fibers with [BMIM]Cl as solvent. By increasing draw ratio, the orientation and crystallinity of the fibers were improved. This resulted in higher tensile strength and initial modulus even though the elongation at break decreased.

Although some engineering problems such as solvent recycling remain unsolved, ILs can be used as direct solvents for cellulose on an industrial scale. The unique characteristics of ILs on regenerated fibers suggest that ILs is very valuable solvents for the dissolution and shaping of cellulose fibers. Spinning of the regenerated cellulose fibers is an area that requires

G. Jiang · Y. Yuan · B. Wang · X. Yin ·  
K. S. Mukuze · W. Huang · Y. Zhang (✉) · H. Wang  
State Key Laboratory for Modification of Chemical Fibers  
and Polymer Materials, Donghua University, Shanghai  
201620, China  
e-mail: zhangym@dhu.edu.cn

further research to improve industrial efficiency. In order to increase productivity of solution spinning, two effective ways can be adopted. These are increasing dope concentration and increasing spinning speed. However, at same spinning conditions the increase of dope concentration is limited by dissolution rate and solution viscosity, which leads to difficulty in filtering and defoaming of the dope. For high-viscosity solutions of cellulose/ILs (Kosan et al. 2008), these problems appear more conspicuous. However, it was found that increasing spinning speed not only increases productivity, but also improves the structure and mechanical properties of fibers. Meng and coworkers (Meng et al. 1998; Meng and Hu 2004) investigated the spinning of Lyocell fibers and concluded that the crystallinity, crystal orientation, birefringence and amorphous orientation of Lyocell fibers increased with increasing spinning speed. As the spinning speed increased to 50 m/min, the birefringence and amorphous orientation of Lyocell fibers reached a maximum. The initial modulus increased even though the elongation at break decreased (Fink et al. 2001; Mortimer and Peguy 1996a, b).

Considering the spinning efficiency of cellulose fibers with ILs as a solvent, the spinning speed was changed in our experiments. The effect of spinning speed on the structure and properties of regenerated cellulose fibers were investigated to illustrate the relationship between the spinning speed and the fiber structure and properties.

## Experimental

### Materials

The cotton pulp ( $DP = 514$ ) was supplied by Shandong Helon Co. Ltd., China. The degree of polymerization of regenerated cellulose fibers and cotton pulp

were estimated by the standard procedure of measuring the intrinsic viscosity  $[\eta]$  in Cuoxam solution by using the empirical relation of  $DP_{\text{Cuoxam}} = 2 [\eta]_{\text{Cuoxam}}$  (Kosan et al. 2008).

[BMIM]Cl was synthesized according to the procedures described by Csihony et al. (2002) in our laboratory.

### Preparation of cellulose/[BMIM]Cl solution

The dried cotton pulp was mixed with [BMIM]Cl at 90 °C in a vacuum with constant stirring in a vertical kneader system until the cellulose pulp was completely dissolved and a homogeneous solutions of 5 wt% were obtained for the spinning process.

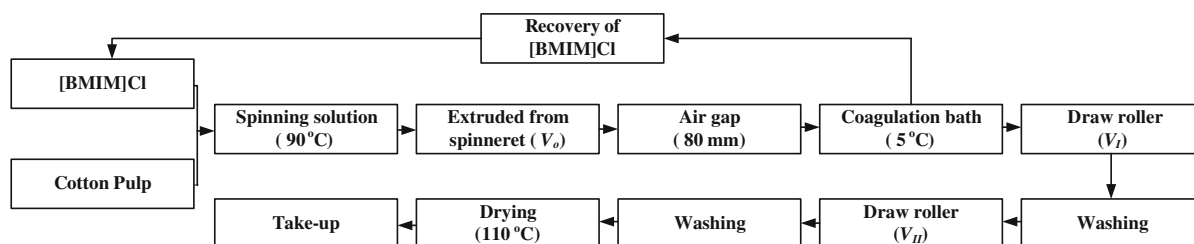
### Preparation of regenerated cellulose fibers

A lab-scale dry–jet–wet spinning experiment was employed to prepare the regenerated cellulose fibers. The technology diagram is shown in Scheme 1. At 90 °C, the spinning solution was extruded through a spinneret which had 40 orifices, and the diameter of the orifice is 0.15 mm. The length of air gap was 80 mm. The conditions used were 65 % relative humidity (RH) at 30 °C.

The coagulation bath had [BMIM]Cl aqueous with a concentration of 10 % and temperature of 5 °C. All filaments were washed with boiling water and dried at 110 °C. The spinning speeds and drawing ratios ( $DR$ ) chosen for regeneration cellulose fibers are listed in Table 1.

### Measurements

The wide-angle X-ray diffraction (WAXD) pattern of the regenerated cellulose fibers was obtained at U7B Beamline station in the National Synchrotron Radiation Laboratory (NSRL) with wavelength of



**Scheme 1** Technology diagram of regenerated cellulose fibers with ILs as solvent

**Table 1** The spinning speeds and drawing ratio (*DR*) chosen for regeneration cellulose fibers

Sample	Extrusion speed $V_0$ (m/min)	First draw speed $V_I$ (m/min)	$DR_I = V_I/V_0$	Second draw speed $V_{II}$ (m/min)	$DR_{II} = V_{II}/V_I$
C1	7.7	38.5	5.0	50.0	1.3
C2	10.0	50.0	5.0	65.0	1.3
C3	12.3	61.5	5.0	80.0	1.3

0.15418 nm and a  $2,300 \times 2,300$  pixels two-dimensional (2D) detector. The distance between sample and detector was set to 140 mm. The exposing time was 180 s. 2D WAXD patterns were processed with the software package FIT2D (Hammersley 1987–1997) to correct for air scattering.

The rheological measurements were carried out on a rotational rheometer (Physica MCR 301, Anton Paar). The concentric parallel plate geometry (diameter: 25 mm) was used for solutions with viscosity above 100 Pa s at 90 °C. For dynamic oscillation, the linear viscoelastic (LVE) region was firstly determined by performing strain sweep with a fixed angular frequency of 6.3 rad/s, then the dynamic frequency sweep measurements were tested within LVE region from angular frequencies 100 to 0.1 rad/s. The temperature control was done by Peltier effect within  $\pm 0.01$  °C of the preset value.

According to the 2D WAXD patterns of powder samples, which were corrected for air scattering, integrated diffraction intensity profile was obtained. The data were analyzed with Peak fit software (version 4.12, Seasoive Co., San Jose, CA). Crystallinity was calculated from Eq. (1):

$$W_{c,x} = \frac{I_c}{I_c + I_a} \times 100\% \tag{1}$$

where  $W_{c,x}$  is the crystallinity,  $I_c$  and  $I_a$  are the total peak area of the crystalline and the amorphous phases, respectively.

The crystallite size of regenerated cellulose fibers was determined from Scherrer Equation (1918):

$$L_{hkl} = \frac{K\lambda}{\beta \cos \theta} \tag{2}$$

where  $L_{hkl}$  is the crystallite size ( $hkl$ ) plane,  $\lambda$  is the wavelength of X-ray,  $\theta$  is half of the diffraction angle ( $2\theta$ ),  $\beta$  is the integral width of the diffraction peak and  $K$  is a constant that is commonly assigned a value of 0.9.

For the fiber with uniaxial orientation, it is better to investigate the orientation degree of crystal molecular

chain axis ( $c$ ) which is along the draw direction ( $Z$ ). The degree of crystal orientation was determined according to the Hermans' orientation function ( $f_c$ ) (Klug and Alexander 1954):

$$f_c = \frac{3\langle \cos^2 \varphi_{c,Z} \rangle - 1}{2} \tag{3}$$

where  $\langle \cos^2 \varphi_{c,Z} \rangle$  is orientation parameter of crystal molecular chain axis ( $c$ ) along the draw direction ( $Z$ ).

The orientation parameter  $\langle \cos^2 \varphi_{c,Z} \rangle$  was determined according to the Wilchinsky Model (1959) and crystal symmetry of regenerated cellulose fibers (Kolpak and Blackwell 1976) with characteristic reflections in equatorial (110), (020) and  $(\bar{1}10)$ . For the reflections ( $hkl$ ), the orientation parameter  $\langle \cos^2 \varphi_{hkl} \rangle$  can be calculated from equation (Klug and Alexander 1954):

$$\langle \cos^2 \varphi_{hkl} \rangle = \frac{\int_0^{\pi/2} I(\varphi_{hkl}) \cos^2 \varphi_{hkl} \sin \varphi_{hkl} d\varphi_{hkl}}{\int_0^{\pi/2} I(\varphi_{hkl}) \sin \varphi_{hkl} d\varphi_{hkl}} \tag{4}$$

where  $\varphi_{hkl}$  represents the azimuthal angle and  $I(\varphi_{hkl})$  is the intensity along the reflection plane ( $hkl$ ). The orientation parameter  $\langle \cos^2 \varphi_{hkl} \rangle$  of regenerated cellulose was evaluated from WAXD 2D detector images according to the method reported in the literature (Gindl et al. 2006).

Birefringence measurements of fibers were performed on an Olympus Co. (Tokyo, Japan) XP51 optical polarized light microscope with the aid of an Olympus CTB Berek compensator. Moreover, the birefringence of regenerated cellulose fibers were calculated from the empirical equation as follows:

$$\Delta n = \frac{\theta \lambda}{180^\circ d} \tag{5}$$

$\lambda = 0.589 \times 10^{-9}$  m;  $\theta$  is the compensatory angle ( $^\circ$ );  $d$  is the diameter of cellulose filament.

The Stein equation was used to determine the amorphous orientation factor ( $f_a$ ):

$$\Delta n = W_{c,x} f_c \Delta n_{co} + (1 - W_{c,x}) f_a \Delta n_{ao} \quad (6)$$

where  $\Delta n$  is the birefringence of regenerated cellulose fibers,  $W_{c,x}$  is the crystallinity,  $\Delta n_{co}$  and  $\Delta n_{ao}$  are the birefringence of the crystalline regions and amorphous regions, respectively, and  $\Delta n_{co} = \Delta n_{ao} = 0.0545$  (Peng et al. 2003).

X-ray scattering (SAXS) profiles were carried out at 16B1 Beamline station in Shanghai Synchrotron Radiation Facility (SSRF). The wavelength was 0.12418 nm. A CCD X-ray detector (MAR CCD 165) was used at a distance of 5053 mm from the sample. Tendon of ox ( $L = 65.8$  nm) was employed for calibration. Software package FIT2D (Hammersley 1987–1997) processed the SAXS 2D images.

For regenerated cellulose fibers, many reports (Statton 1956; Crawshaw and Cameron 2000; Vickers et al. 2001; Chen et al. 2006, 2007) have indicated that the streak on the equator in the SAXS of regenerated cellulose fibers is attributed to the scattering of the needle-shaped microvoids along the fiber direction. Therefore, radius of microvoids with circles cross-section can be described by Guinier functions, shown in Eq. (7) (Guinier and Fournet 1955):

$$I(q) = I(0) \exp\left(\frac{-q^2 R^2}{5}\right) \quad (7)$$

where  $R$  is the radius of microvoids with circles cross section,  $q$  ( $q = 4\pi \sin \theta/\lambda$ ) is the scattering vector,  $2\theta$  is the scattering angle and  $\lambda$  is the wavelength.

And the average microvoids length ( $L$ ) and misorientation ( $B_\phi$ ) which is parallel to the fiber axis were determined by the method of Ruland (Ruland 1969).

Mechanical tests were carried out with material testing equipment (XQ-1, China) at least ten standard tensile specimens were tested for each series. The drawing speed was 20 mm/min.

## Results and discussion

### Rheological behavior of the cellulose/[BMIM]Cl solution

The rheological property of the cellulose solution is an extremely important factor in the shaping process, the structure formation, and the properties of cellulose fibers prepared by the ILs methods (Kosan et al. 2008). Figure 1 shows the master curves of cellulose solution

in [BMIM]Cl with concentration of 5 % at 90 °C. The complex viscosity of the solution obviously decreased with an increase in angular frequency ( $\omega$ ), showing a typical shear-thinning behavior. Moreover, the complex viscosity of the cellulose/[BMIM]Cl solution with concentration of 5 % at 90 °C can be determined from the Fig. 1, approximately 50 (Pa s), implying the system could be spun easily around this temperature. The solution can be appropriately characterized by the determination of Loss modulus and storage modulus are plotted against frequency as shown in Fig. 1. In a previous publication (Chen et al. 2011), we discussed that time–temperature superposition worked very nicely for the linear viscoelastic oscillatory shear response of cellulose/[BMIM]Cl solutions, the entanglement of internal molecule of solution system could be observed while the concentration of cellulose/[BMIM]Cl exceed the 4 %. This indicated that above this concentration can be good used to spinning the regenerated cellulose fibers.

### Mechanical properties of the regenerated cellulose fibers spun at different spinning speed

In order to avoid the effect of other technologies such as drawing ratio on the structure and mechanical properties of regenerated cellulose fibers during manufacturing. In this work, as shown in Table 1, the samples were prepared with drawing ratios at different spinning speeds. The mechanical properties of regenerated cellulose fibers at different spinning speed are shown in Table 2. The tenacity and modulus of regenerated cellulose fibers increased with the spinning speed. The draw ratio was kept constant and

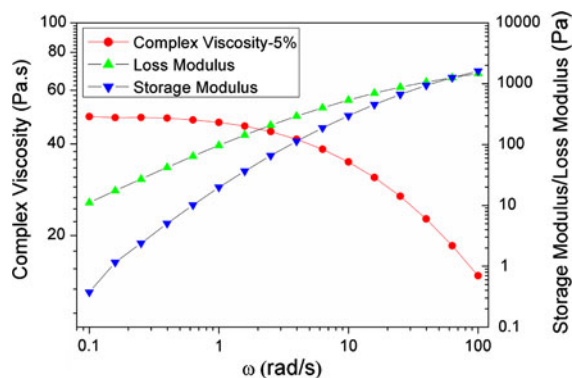


**Fig. 1** Master curves of solutions of cotton pulp ( $DP = 514$ ) in [BMIM]Cl with concentration of 5 % at 90 °C

**Table 2** The mechanical properties of regenerated cellulose fibers spun at different spinning speed

Sample	C1	C2	C3
Linear density (dtex)	2.22	2.22	2.22
Initial modulus (0.5–0.9 %) (cN/dtex)	63.8	71.2	72.5
Elongation at break (%)	6.6	6.5	6.2
Tenacity (dry) (cN/dtex)	3.51	3.88	4.21

the elongation at break decreased slightly. Surprisingly, the tenacity and modulus of regenerated cellulose fibers with [BMIM]Cl as solvent is apparently higher than that of the Viscose fibers, this results consists with the previous report (Jiang et al. 2012). Kosan et al. (2008) concluded that the regenerated cellulose fibers spun from [BMIM]Cl solutions shown a higher tenacities but lower values for the elongation than fibers with NMMO as solvent. Above description suggests that the mechanical properties of the regenerated cellulose fibers with ILs as solvents not only can be optimized by adjusting spinning speed, but also a higher efficiency of regenerated cellulose fibers spinning process with [BMIM]Cl as a solvent is connected with an increase of the tenacity values of the spun fibers.

#### Crystalline structure of regenerated cellulose fibers spun at different spinning speed

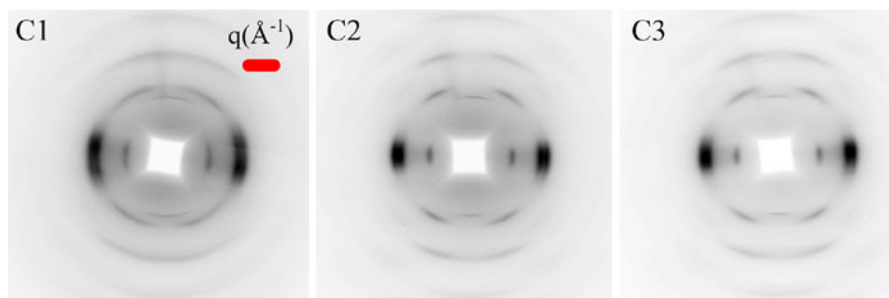
The crystal parameters of regenerated cellulose fibers spun at different spinning speed were analyzed according to 2D WAXD patterns shown in Fig. 2. A typical cellulose II crystalline structure with a monoclinic unit cell (Langan et al. 2001) is shown in the diffraction pattern with the characteristic reflections ( $\bar{1}10$ ), (110) and (020) on the equator and the

(002) reflection in meridian, just like that of Lyocell fibers (Jiang et al. 2012). Although the formation of the crystalline structure of regenerated cellulose fibers during the preparation process was independent on the spinning technology, the width and length of the reflection arc are different from the spinning technology. From Fig. 2, although the WAXD patterns of the three samples were very similar, shorter arcs appeared as spinning speed increased. This indicates that the increasing spinning speed causes better crystal orientation in the axial direction, resulting in regenerated cellulose fibers showing a higher degree of orientation and crystallinity.

According to the cellulose II crystalline structure, six main reflection peaks and an amorphous peak were employed to fit the experimental data as illustrated in Fig. 3. Subsequently, the crystallinity and crystal size of three samples were determined and listed in Table 3. It was found that the crystal size changed slightly with the spinning speed and the crystallinity of fibers also increased with increasing spinning speed. The degree of crystal orientation ( $f_c$ ), amorphous orientation factor ( $f_a$ ) and birefringence ( $\Delta n$ ) were also calculated and given in Table 3. The increase in spinning speed also increased the degree of crystal orientation and the amorphous orientation of regenerated cellulose fibers as well as the birefringence of fibers. With the higher spinning speed made the cellulose molecules more easily align to form an ordered structure. And the higher crystallinity of regenerated cellulose fibers was induced by the higher orientation.

#### Micromorphology of regenerated cellulose fibers spun at different spinning speed

The microvoids in regenerated cellulose fibers spun at different spinning speed were analyzed by SAXS,

**Fig. 2** WAXD patterns of regenerated cellulose fibers spun at different spinning speed: C1 50 m/min, C2 65 m/min, and C3 80 m/min



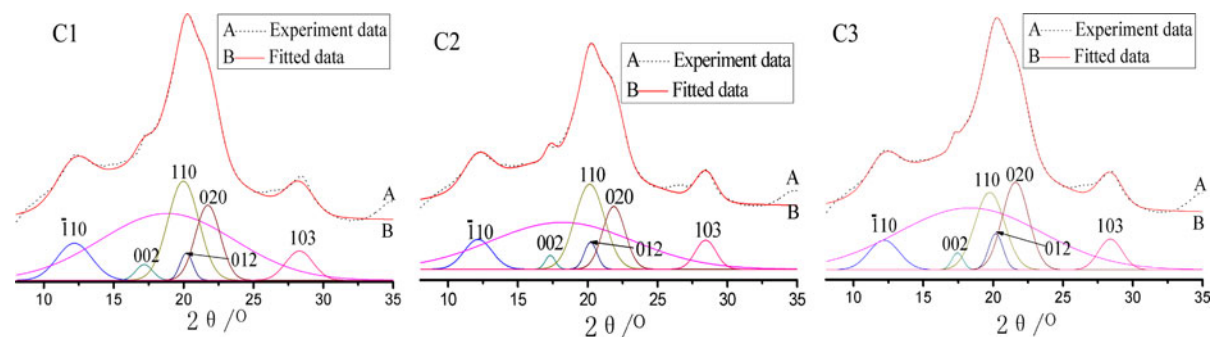


**Fig. 3** One-dimensional integrated WAXD intensity profile of powder samples of the regenerated fibers spun at different spinning speed and the corresponding peak deconvolution

process to calculate the crystallinity and crystal size: **C1** 50 m/min, **C2** 65 m/min, and **C3** 80 m/min

**Table 3** Crystal size, crystallinity, degree of crystal orientation ( $f_c$ ), amorphous orientation factor ( $f_a$ ) and birefringence ( $\Delta n$ ) of the regenerated cellulose fibers spun at different spinning speed

Sample	Crystal size ( $\text{\AA}$ )						Crystallinity (%)	Crystal orientation $f_c$ (%)	Amorphous orientation factor $f_a$ (%)	Birefringence $\Delta n \times 10^2$
	( $\bar{1}10$ )	(002)	(110)	(012)	(020)	(103)				
C1	35.3	35.1	35.4	74.5	34.3	35.5	67	74.1	74.5	2.65
C2	35.5	36.2	36.0	83.1	35.3	36.6	72	82.7	83.1	2.82
C3	37.3	37.2	37.1	83.4	36.2	36.8	73	83.0	83.4	2.86

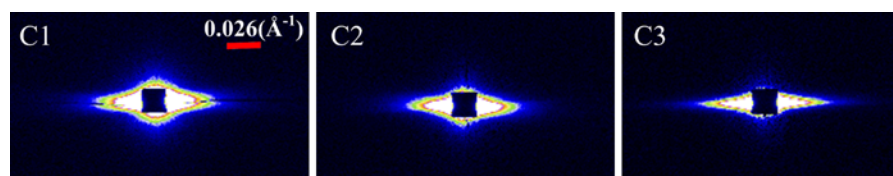


**Fig. 4** SAXS patterns of regenerated cellulose fibers at different spinning speed: **C1** 50 m/min, **C2** 65 m/min, and **C3** 80 m/min

shown in Fig. 4. The SAXS patterns showed a sharp and elongated equatorial streak in intensity, which was considered as the scattering by long thin voids parallel to the fiber axis (Statton 1956; Perret and Ruland 1969; Saijo et al. 1994; Crawshaw and Cameron 2000; Moss et al. 2002; Vickers et al. 2001; Chen et al. 2006, 2007). Moreover, in Fig. 4 (C1 and C2), the SAXS patterns exhibit relatively weak and short meridional streak, which is attributed to the decrease of microvoids orientation and microvoids length in cellulose fibers (Ruland 1969; Wang et al. 1993).

The Guinier plots of the scattered intensities along the equatorial streak ( $q = 0 \text{ \AA}^{-1}$ ) in the horizontal direction were obtained, subsequently the tangent curve of Guinier plot also determined. The Guinier plots were subtracted by the tangent curve and formed

new values. A repeat of the above procedure was done according to the tangent method shown in Fig. 5. Figure 5 shows a typical polydisperse system and an analysis for these results can be made by resolving the curve into successive tangents (Statton 1956; Fischer et al. 1978). The sizes of the microvoids located at cross-section of regenerated cellulose fibers were calculated by Eq. (7) and the result is listed in Table 4. The regenerated cellulose fibers show microvoids characteristics with multi-order cross-section. The size of voids in the cross-section decreased with increasing spinning speed.

Figures 6 and 8 show the azimuthal scans of sample C1 extracted at different scattering vectors and the Ruland plot for the regenerated cellulose fibers spun at different spinning speeds, respectively. As shown in

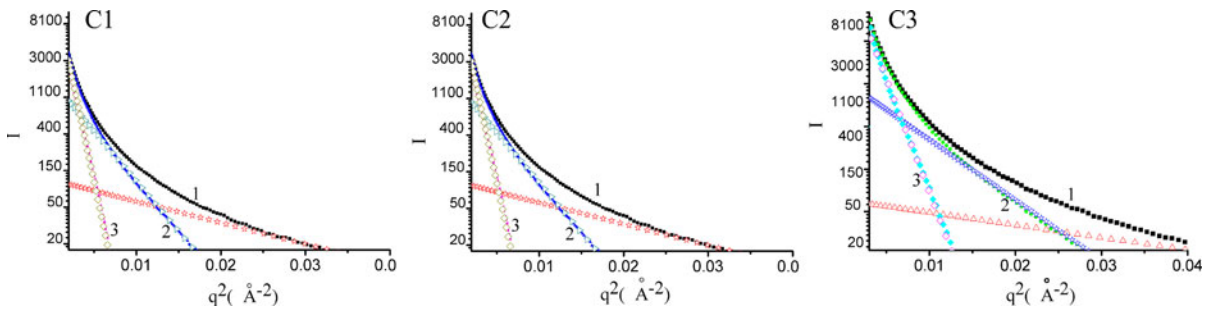


**Fig. 5** Guinier plot of the scattered intensities along the layer line ( $q = 0 \text{ \AA}^{-1}$ ) in the horizontal direction. 1 = measured values, 2 = values after subtracting the resolved curve 1, 3 = values after subtracting the resolved curve 1 and 2: **C1** 50 m/min, **C2** 65 m/min, and **C3** 80 m/min

**Table 4** The microvoids parameters of the regenerated cellulose fibers spun at different spinning speed

Sample	$R_1$ (Å)	$R_2$ (Å)	$R_3$ (Å)	Microvoids length $L$ (Å)	Misorientation $B_\Phi$ (°)
C1	17.1	36.9	73.9	4040	14.6
C2	12.9	28.4	53.3	4415	13.4
C3	12.1	26.6	51.5	5215	10.9

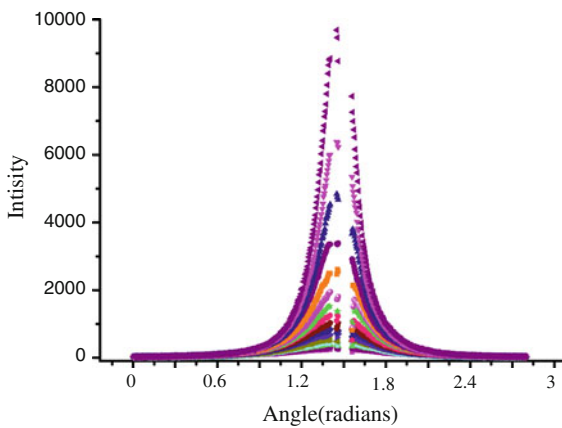


**Fig. 6** Azimuthal scans at different vales of regenerated cellulose fibers from the sample **C1** in Fig. 4

Fig. 7, the peak profiles from azimuthal scans of the equatorial streak of regenerated cellulose fibers are better fitted with Lorentzian function, expressed as Eq. (8):

$$sB_{\text{obs}} = \frac{1}{L} + sB_\Phi \quad \text{Cauchy - Cauchy} \quad (8)$$

where  $B_{\text{obs}}$  is the full width at half maximum of the azimuthal profile from the equatorial streak fitted with a Lorentzian function;  $s = 2 \sin \theta / \lambda$ ,  $2\theta$  is the scattering angle and  $\lambda$  is X-ray wavelength.

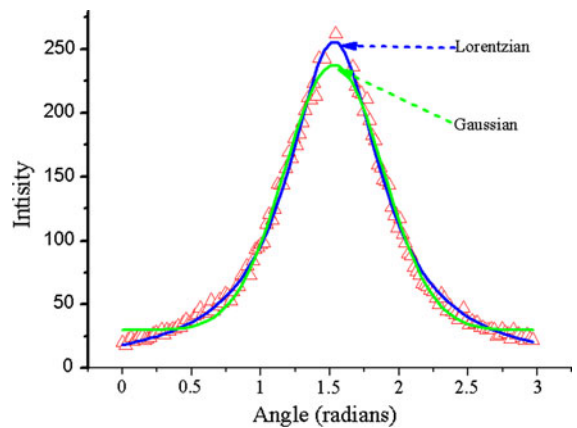


**Fig. 7** Representative azimuthal scans of the equatorial streak from the sample **C1**. The *trigon* represents the experimental data, the *blue* and *green* line corresponds to the Lorentzian and Gaussian fit, respectively

The results are shown in Table 4. By increasing spinning speed, the length of the microvoids increased as 4040, 4415 and 5215 Å, corresponding to the spinning speed of 50, 65 and 80 m/min respectively. Consequently the microvoids misorientation from the fiber axis greatly decreased with increasing spinning speed. This result is consistent with the results of crystalline orientation (Fig. 2).

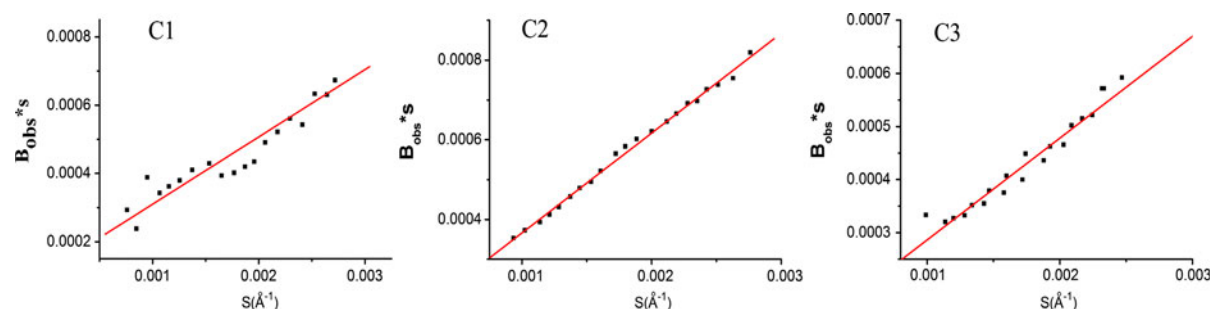


**Fig. 8** Ruland plot of regenerated cellulose fibers spun at different spinning speed: **C1** 50 m/min, **C2** 65 m/min, and **C3** 80 m/min

### Analysis of spinline stress of regenerated cellulose fibers at different spinning speed

From the above analysis, it is clear that the mechanical properties and structure depend largely on spinning speed. The spinline stress is analyzed to understand why the mechanical and structure changed with the spinning speed.

The stress ( $F_{rheo}$ ) on spinline can be described as following (Salem 2004):

$$F_{rheo} = F_o + F_{inert} + F_{surf} + F_{drag} - F_{grav} \quad (9)$$

where  $F_{rheo}$  is the rheological resistance of cellulose filament on spinline.  $F_o$  is the rheological resistance of cellulose filament at spinning nozzle.  $F_{inert}$  is inertia force overcome by spinning line as it moves with axial acceleration.  $F_{surf}$  is the surface tension overcome by spinning line during the spinning process.  $F_{drag}$  is the friction generated by media on the surface of moving spinning line.  $F_{grav}$  is the force of gravity field on spinning line. During the process of dry–jet–wet spinning, the values of  $F_{grav}$  and  $F_{surf}$  are small so these can be completely ignored. The  $F_{inert}$  increases with the difference between spinning speed ( $V_1$ ) and extrusion speed ( $V_0$ ): the larger the difference of absolute value of spinning speed, the larger the inertia force. Moreover, the shear stress that the coagulation bath is exerting on the surface of filaments is proportional to the square of spinning speed, suggesting that the larger the absolute value of spinning speed the larger the value for  $F_{drag}$ . In addition, the  $F_o$  of filaments is also proportional to the velocity gradient of the spinneret in the direction of axis (shown in Table 1). Therefore the increase of spinning speeds not only leads to enhancement of velocity gradient, but also results in the rheological resistance of filaments being increased. Due to the spinning speed being

proportional to the velocity gradient of the filament, raising the  $F_{rheo}$  by increasing spinning speeds means that spinline stress is increased.

From the above analysis, increasing spinning speed increases spinline stress resulting in an increase in the orientation and crystallinity of the cellulose fibers. This leads to increased tenacity and initial modulus of the fibers. At the same time, the spinning efficiency is also increased.

### Conclusion

With higher spinning speeds, the spinline stress increases, resulting in the increase of capacity as well as tenacity of the regenerated cellulose fibers spun with IL as a solvent. From the analysis of the crystalline structure and micromorphology of regenerated cellulose fibers, it is shown that the crystallinity, birefringence, crystal and microvoid orientation improved as spinning speed increased contributing to the mechanical properties of the fibers.

**Acknowledgments** The work was supported by a grant from National Natural Science Foundation of China (50873025), Shanghai Leading Academic Discipline Project (B603), the Innovation Funds for PhD Students (Jiang Guansen) of Donghua University, and Basal Research Operation Cost Special Foundation of Central University. WAXD and SAXS experiments were performed at U7B Beamline station in the National Synchrotron Radiation Laboratory (NSRL) and 16B1 Beamline station in Shanghai Synchrotron Radiation Facility (SSRF), respectively.

### References

- Cai T, Zhang HH, Guo QH, Shao HL, Hu XC (2010) Structure and properties of cellulose fibers from ionic liquids. *J Appl Polym Sci* 115:1047–1053



- Chen XM, Burger C, Fang DF, Ruan D, Zhang LN, Hsiao BS, Chu B (2006) X-ray studies of regenerated cellulose fibers wet spun from cotton linter pulp in NaOH/thiourea aqueous solutions. *Polymer* 47:2839–2848
- Chen XM, Burger C, Wan F, Zhang J, Rong LX, Hsiao BS, Chu B, Cai J, Zhang LN (2007) Structure study of cellulose fibers wet-spun from environmentally friendly NaOH/urea aqueous solutions. *Biomacromolecules* 8:1918–1926
- Chen X, Zhang YM, Wang HP (2011) Solution rheology of cellulose in 1-butyl-3-methylimidazolium chloride. *J Rheol* 55:485–494
- Crawshaw J, Cameron RE (2000) A small angle X-ray scattering study of pore structure in Tencel cellulose fibres and the effects of physical treatments. *Polymer* 41:4691–4698
- Csihony S, Fischmeister C, Bruneau C, Horváth I, Dixneuf P (2002) First ring-opening metathesis polymerization in an ionic liquid. Efficient recycling of a catalyst generated from a cationic ruthenium allenylidene complex. *New J Chem* 11:1667–1670
- Cuissinat C, Navard P, Heinze T (2008) Swelling and dissolution of cellulose. Part IV: free floating cotton and wood fibres in ionic liquids. *Carbohyd Polym* 72:590–596
- Fink H, Weigel P, Purz H, Ganster J (2001) Structure formation of regenerated cellulose materials from NMMO-solutions. *Prog Polym Sci* 26:1473–1524
- Fischer EW, Herchenroder P, Manley RSJ, Stamm M (1978) Small-angle neutron scattering of selectively deuterated cellulose. *Macromolecules* 11:213–217
- Gindl W, Martinschitz KJ, Boesecke P, Keckes J (2006) Orientation of cellulose crystallites in regenerated cellulose fibres under tensile and bending loads. *Cellulose* 13:621–627
- Guinier A, Fournet G (1955) *Small-angle scattering of X-rays*. Wiley, New York
- Hammersley (1987–1997) A FIT2D 2-D detector calibration/correction; file re-formatting; 2-D fitting; European Synchrotron Radiation Facility (ESRF)
- Hermanutz F, Meister F, Uerdingen E (2006) New developments in the manufacture of cellulose fibers with ionic liquids. *Chem Fiber Int* 6:342–343
- Jiang G, Huang W, Li L, Wang X, Pang F, Zhang Y, Wang H (2012) Structure and properties of regenerated cellulose fibers from different spinning technologies. *Carbohyd Polym* 87:2012–2018
- Klug H, Alexander L (1954) *X-ray diffraction procedures*. Wiley, New York
- Kolpak FJ, Blackwell J (1976) Determination of the structure of cellulose II. *Macromolecules* 9:273–278
- Kosan B, Michels V, Meister F (2008) Dissolution and forming of cellulose with ionic liquids. *Cellulose* 15:59–66
- Langan P, Nishiyama Y, Chanzy H (2001) X-ray structure of mercerized cellulose II at 1 Å resolution. *Biomacromolecules* 2:410–416
- Laus G, Bentivoglio G, Schottenberger H, Kahlenberg V, Kopacka H, Röder T, Sixta H (2005) Ionic liquids: Current developments, potential and drawbacks for industrial applications. *Lenzinger Berichte* 84:71–85
- Meng Z, Hu X (2004) Effects of spinning speed on structure of Lyocell fiber. *Journal of Henan Normal University* 32: 74–77
- Meng Z, Hu X, Zhang T (1998) The influence of air-gap length and spinning speed on the mechanical properties of Lyocell fiber. *Syn fiber* 27:7–10
- Mortimer S, Peguy A (1996a) The formation of structure in the spinning and coagulation of Lyocell fibers. *Cell Chem Tech* 30:117–132
- Mortimer S, Peguy A (1996b) The influence of air-gap conditions on the structure formation of Lyocell fibers. *J Appl Polym Sci* 60:1747–1756
- Moss CE, Butler MF, Muller M, Cameron RE (2002) Micro-focus small-angle X-ray scattering investigation of the skin-core microstructure of Lyocell cellulose fibers. *J Appl Polym Sci* 83:2799–2816
- Peng S, Shao H, Hu X (2003) Lyocell fibers as the precursor of carbon fibers. *J Appl Polym Sci* 90:1941–1947
- Perret R, Ruland W (1969) Single and multiple X-ray small-angle scattering of carbon fibers. *J Appl Crystallogr* 2:209–218
- Ruland W (1969) Small-angle scattering studies on carbonized cellulose fibers. *J Polym Sci Polym Symp* 1:143–151
- Saijo K, Arimoto O, Hashimoto T, Fukuda M, Kawai H (1994) Moisture sorption mechanism of aromatic polyamide fibres: Diffusion of moisture into regular Kevlar as observed by time-resolved small-angle X-ray scattering technique. *Polymer* 35:496–503
- Salem DR (2004) *Structure formation in polymeric fibers*. Chemistry Industry Press, Peking
- Scherrer P (1918) Bestimmung der grosse und der inneren struktur von Kolloidteilchen mittels rontgenstrahlen. *Gottinger Nachr. Math Phys* 2:98–100
- Statton WO (1956) Crystallite regularity and void content in cellulose fibers as shown by small-angle X-ray scattering. *J Polym Sci* 22:385–397
- Swatloski RP, Spear SK, Holbrey JD, Rogers RD (2002) Dissolution of cellulose with ionic liquids. *J Am Chem Soc* 124:4974–4975
- Vickers ME, Briggs NP, Ibbett RN, Payne JJ, Smith SB (2001) Small angle X-ray scattering studies on Lyocell cellulosic fiber: The effects of drying, re-wetting and changing coagulation temperature. *Polymer* 42:8241–8248
- Wang W, Ruland W, Cohen Y (1993) Fibrillar and microfibrillar structures in poly (p-phenylene terephthalamide) fibers. *Acta Polym* 44:273–278
- Wilchinsky ZW (1959) Advance in X-ray analysis. *J Appl Phys* 30:782–789